

Evolution of transport and magnetic properties near the ferromagnetic quantum critical point in the series $\text{Ca}_x\text{Sr}_{1-x}\text{RuO}_3$

P. Khalifah, I. Ohkubo, H. M. Christen, and D. G. Mandrus

Oak Ridge National Laboratory, Condensed Matter Sciences Division, Oak Ridge, Tennessee 37831, USA

(Received 13 July 2004; revised manuscript received 26 July 2004; published 29 October 2004)

A series of epitaxial films were grown across the solid solution $\text{Ca}_x\text{Sr}_{1-x}\text{RuO}_3$ in order to pinpoint the ferromagnetic to paramagnetic quantum phase transition in this system and to study the evolution of transport and magnetic properties in its vicinity. The ferromagnetic T_c of SrRuO_3 was found to decrease linearly with Ca doping levels up to 70%. Further doping resulted in the abrupt elimination of ferromagnetic order, and the onset of low temperature (<10 K) non-Fermi-liquid (NFL) resistivity of the form $\rho \propto \rho_0 + AT^{1.5}$ for samples with $x \leq 0.75 \leq 1.0$. The resistivity exponent of 1.5 matches that previously observed for intermetallic alloys (such as MnSi) at their ferromagnetic quantum critical points, indicating the possible universality of this NFL behavior. Field-dependent specific heat measurements on bulk samples at compositions near the quantum phase transition provide additional evidence for NFL behavior ($C/T \propto \log_{10} T$) and show the conditions under which spin fluctuations contribute to the specific heat.

DOI: 10.1103/PhysRevB.70.134426

PACS number(s): 72.15.Eb, 75.30.Kz, 75.40.-s

Ruthenates initially attracted the attention of the physics community when superconductivity was discovered in Sr_2RuO_4 ,¹ a compound isostructural with the high- T_c superconductor $\text{La}_{2-x}\text{Ba}_x\text{CuO}_4$.² Since that time, ruthenates have proved to be interesting in their own right, with their 4d magnetism³⁻⁶ generating as much or more interest than their superconductivity. A focus area of ruthenate research which draws on both their good conductivity and their tunable magnetism has recently emerged, converging in the study of non-Fermi-liquid (NFL) behavior in these systems.^{3,4,7,8} The Fermi-liquid model of Landau predicts a standard behavior of metallic systems at low temperatures, namely a resistivity ρ which scales as T^2 , a temperature independent magnetic susceptibility χ , and a temperature-normalized specific heat C/T which is constant. The preconditions of this model (T -independent electron interactions which are short range in both space and time⁹) are almost universally satisfied among solid state compounds. The compounds which are the exception to this rule (non-Fermi-liquids, or NFL materials) are therefore of interest. The study of NFL compounds had its genesis with $\text{U}_x\text{Y}_{1-x}\text{Pd}_3$,¹⁰ and has now been extended to a few dozen intermetallic systems.⁹ NFL behavior in oxides remains rare, and the best examples to date have been found among ruthenates, most notably $\text{La}_4\text{Ru}_6\text{O}_{19}$,³ $\text{Sr}_3\text{Ru}_2\text{O}_7$,⁴ and CaRuO_3 .⁷

One potential route for finding NFL behavior is tuning a system to the vicinity of a quantum phase transition (QPT), a regime where the length scale of electronic fluctuations are diverging as the precise end point of the quantum phase transition is approached. This methodology has been used to study NFL behavior in systems such as $\text{U}_x\text{Y}_{1-x}\text{Pd}_3$ (Ref. 10) and $\text{CeCu}_{6-x}\text{Au}_x$ (Ref. 11), whose antiferromagnetic ordering temperature T_N can be suppressed to zero by doping. Additionally, NFL behavior can be found at a metamagnetic transition, as exemplified on the field-tuning experiments on $\text{Sr}_3\text{Ru}_2\text{O}_7$.⁴ Similar behavior can be found by suppressing the Curie temperature (T_c) of ferromagnets, as was observed when hydrostatic pressure was applied to suppress the weak

ferromagnetism of MnSi.^{12,13} Of these three routes to QPT's, those involving ferromagnetic QPT's are the rarest,⁹ and the discovery and characterization of additional systems with ferromagnetic QPT's will provide essential information for the study of NFL quantum criticality.

The perovskite $\text{Ca}_x\text{Sr}_{1-x}\text{RuO}_3$ series is a good candidate system for observing NFL behavior at the vicinity of a ferromagnetic quantum critical point, given that SrRuO_3 is a moderately strong itinerant electron ferromagnet ($T_c = 160$ K) whose T_c can be completely suppressed via Ca substitution. This system has been shown to be metallic across its entire breadth.¹⁴ Furthermore, studies on epitaxial films of its end member CaRuO_3 have found a resistivity exponent of $\rho \propto \rho_0 + AT^{1.5}$.^{7,8} Specific heat studies on powder samples have found a diverging C/T near a Ca content of $x=0.8$.¹⁵ As powder samples are unsuitable for measuring resistivity exponents, and no method exists for synthesizing precisely targeted compositions of $\text{Ca}_x\text{Sr}_{1-x}\text{RuO}_3$ crystals, this study examined the resistivity of thin film samples in the $\text{Ca}_x\text{Sr}_{1-x}\text{RuO}_3$ series. In addition, a select set of powder samples with a composition near $x=0.8$ was prepared to study the field-dependent behavior of the specific heat near the critical regime.

$\text{Ca}_x\text{Sr}_{1-x}\text{RuO}_3$ films were grown epitaxially on a lanthanum aluminum oxide (LAO) substrate using a two-target pulsed laser deposition technique. The two targets of commercially obtained SrRuO_3 and CaRuO_3 (Praxair) were mounted on a rotating carousel, and by varying the relative number of laser pulses fired onto each target the stoichiometry of the film could be precisely controlled. For all mixed samples, the maximum number of pulses fired consecutively on one target was always less than 10 (note that 25 pulses are typically necessary to deposit a full perovskite monolayer). For film growth, the substrates were mounted on a heated plate that was kept at 675 °C in a background of 80 mTorr of oxygen. KrF (248 nm) excimer radiation was used with an energy density of 3.87 J/cm² at the target. The thicknesses of the films were measured by cross-sectional scanning electron

microscopy (SEM) analysis, and were approximately 2000 Å in height. Film compositions were monitored both by energy dispersive x-ray analysis (EDX) and Rutherford backscattering (RBS).

Powder $\text{Ca}_x\text{Sr}_{1-x}\text{RuO}_3$ samples for heat capacity measurements were prepared from high purity starting reagents of RuO_2 (Alfa, 99.95%), SrCO_3 (Alfa, 99.995%), and CaCO_3 (Alfa, 99.995%). Ground mixtures of the stoichiometric ratios of the reagents (with 1 mol % excess RuO_2) were initially calcined at 1100 °C to react ruthenium with the carbonates, minimizing the Ru volatility in future heating steps. The product of this reaction was phase separated into Ca-rich and Sr-rich perovskite fractions, as seen in powder x-ray diffraction patterns collected on a Scintag PAD-V diffractometer. Further grinding and heat treatments (~48 h total) at 1300 °C were necessary to obtain a single perovskite phase. Isostatically pressed pellets (1/2 in. diameter, 2 tons pressure) were then prepared and fired at 1300 °C. Small sections were cut from these dense pellets to use in heat capacity measurements.

Sample resistivities were measured using four-probe measurements on bar samples with areas of approximately $1 \times 4 \text{ mm}^2$. Pt wire leads (1 mil) were attached using silver epoxy (Epotek, H20E). A short (~1 h) high temperature anneal (300–500 °C) was necessary to reduce the contact resistance below 5 Ω. The dc resistance and magnetoresistance measurements were done in the 2–350 K temperature range in a Quantum Design Physical Property Measurement System (PPMS) using a sufficiently low current (typically 0.5 to 5.0 mA) to avoid sample heating. Magnetoresistance measurements were made on heating after previously cooling samples in the absence of a magnetic field. Residual resistivities were on the order of 50–150 $\mu\Omega \text{ cm}$ while room temperature resistivities fell between 150 and 400 $\mu\Omega \text{ cm}$. Heat capacity measurements were performed in the Quantum Design PPMS using dense plates of pressed powder samples with typical masses of 30–45 mg cut from the center of pellets. Magnetic measurements were performed in a commercial magnetometer (Quantum Design MPMS).

The primary advantage of thin film resistivity measurements over single crystal measurements in the $\text{Ca}_x\text{Sr}_{1-x}\text{RuO}_3$ solid solution is the precise control of sample stoichiometries. Due to the different partition coefficients and different volatilities of CaRuO_3 and SrRuO_3 , the growth of homogeneous mixed $\text{Ca}_x\text{Sr}_{1-x}\text{RuO}_3$ ruthenate perovskites crystals presents a tremendous technical challenge. In contrast, it is a facile process to accurately synthesize targeted compositions of $\text{Ca}_x\text{Sr}_{1-x}\text{RuO}_3$ thin films using our two-target pulsed laser deposition (PLD) process. In this study, the $\text{Ca}_x\text{Sr}_{1-x}\text{RuO}_3$ composition was varied in 10% steps across the entire compositional regime, with one additional sample containing 75% Ca made to allow a finer mesh near the hypothesized quantum phase transition in this system. As can be seen in Fig. 1(a), the targeted and measured composition of all the films were identical within the precision of the measurement techniques.

An additional measure of film quality is the residual resistivity ratio (RRR), here taken to be the resistivity at room temperature divided by the resistivity at 4 K. It can be seen in Fig. 1(b) that the $\text{Ca}_x\text{Sr}_{1-x}\text{RuO}_3$ films typically have good

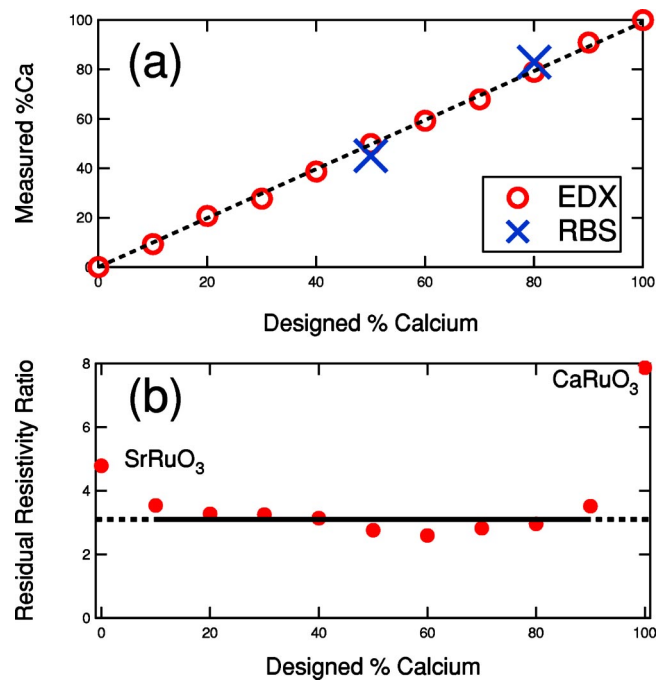


FIG. 1. (Color online) Target and actual compositions of $\text{Ca}_x\text{Sr}_{1-x}\text{RuO}_3$ films as measured by elemental dispersive x-ray analysis (EDX, circles) and Rutherford backscattering (RBS, crosses). (b) Residual resistivity ratios (RRR's) of $\text{Ca}_x\text{Sr}_{1-x}\text{RuO}_3$ films.

RRR's of ~3, with the SrRuO_3 and CaRuO_3 end members having extra high RRR's of 5 and 8, respectively. The lack of composition dependence across the mixed $\text{Ca}_x\text{Sr}_{1-x}\text{RuO}_3$ samples indicates that the reduced RRR's of the quaternary oxides is a result of electronic inhomogeneity (from the presence of two different types of alkali earth sites) rather than strict compositional disorder. A similar trend has been observed in mixed $\text{Ca}_x\text{Sr}_{1-x}\text{RuO}_3$ single crystals.¹⁶ The RRR's of these samples measured here are comparable to those of most previous preparations of CaRuO_3 and SrRuO_3 ,^{14,17} though we note that others have produced some exceptionally high quality films by utilizing chemical vapor deposition (CVD) techniques on strontium titanate (STO) substrates.^{15,18,19}

Our first goal was to accurately determine the composition at which the ferromagnetism of SrRuO_3 is completely suppressed via Ca doping. Magnetic susceptibility measurements [Fig. 2(a)] show that samples with 60% and 70% Ca have substantial magnetic hysteresis, while the sample with 75% Ca does not, placing the end point of this quantum phase transition between $x=0.70$ and $x=0.75$. Due to the small mass of the deposited films (~1 μg), it was impractical to determine the ferromagnetic ordering temperatures from dc susceptibility measurements. Instead, ordering temperatures were obtained from magnetoresistance (MR) measurements, as shown in Fig. 2(b). Each ferromagnetic sample has a well-defined peak. Gaussian fits accurately described the peak maxima, allowing a ferromagnetic T_c to be determined for each sample in the range $0 \leq x \leq 0.70$. It should be noted that the T_c obtained from MR measurements is analogous to T_c obtained from ac magnetic susceptibility measure-

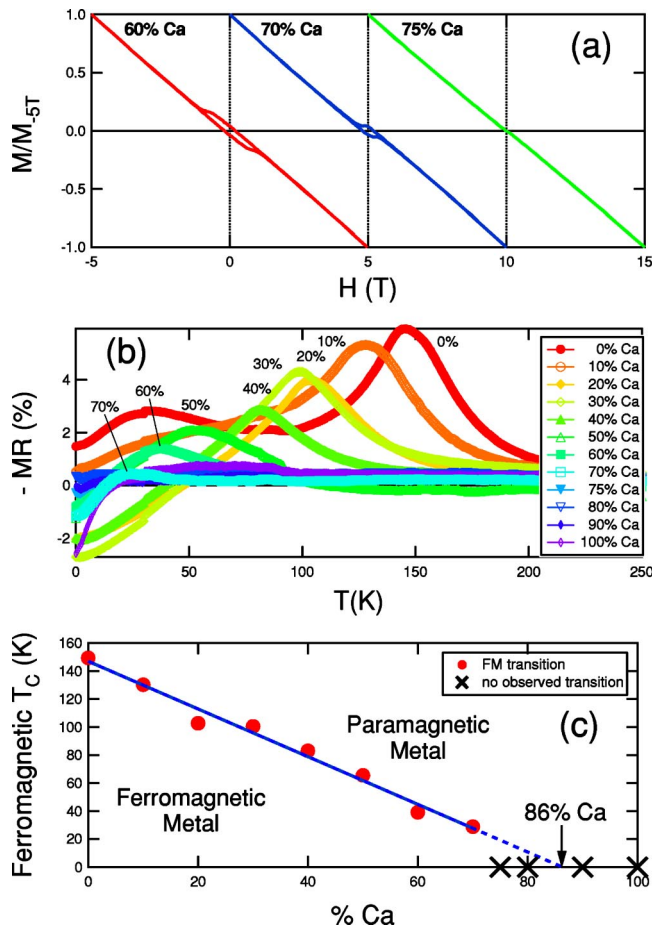


FIG. 2. (Color online) (a) SQUID measurements of $x=0.60, 0.70,$ and $0.75,$ at $T=5$ K. (b) Compositional dependence of magnetoresistance ($\rho_{0T}-\rho_{8T}$). The break in the data sets at 30 K is an artifact of the slower ramp rate used below 30 K. (c) Ferromagnetic phase diagram of $\text{Ca}_x\text{Sr}_{1-x}\text{RuO}_3$ films.

ments. In both of these cases, the peak maximum occurs at the midpoint of the transition where spin fluctuations are largest. This T_c is always lower than the onset T_c obtained from dc magnetic susceptibility measurements.

The ferromagnetic phase diagram of $\text{Ca}_x\text{Sr}_{1-x}\text{RuO}_3$ [Fig. 2(c)] shows a linear dependence of T_c on composition down to 70% Ca. If this line is extrapolated to $T_c=0$, an end point is predicted at $x=0.86$. This is in contrast to both the SQUID and MR measurements, which show that the ferromagnetic ordering disappears by $x=0.75$. It appears that there is a precipitous drop in the ferromagnetic T_c in the vicinity of the $\text{Ca}_x\text{Sr}_{1-x}\text{RuO}_3$ quantum phase transition. The origin of this abrupt change is not known, but will be the focus of future experiments using a finer compositional grid near the transition temperature.

The effect of ferromagnetism on the resistivity of $\text{Ca}_x\text{Sr}_{1-x}\text{RuO}_3$ can be seen in Fig. 3(a), which shows the normalized resistivity of samples with 0–70 % Ca. The high-temperature resistivity data show little compositional variation, though at lower temperatures each of these ferromagnetic samples shows a marked reduction in the resistivity on passing through the magnetic ordering transition due to the reduced spin scattering in the ordered phase. As expected,

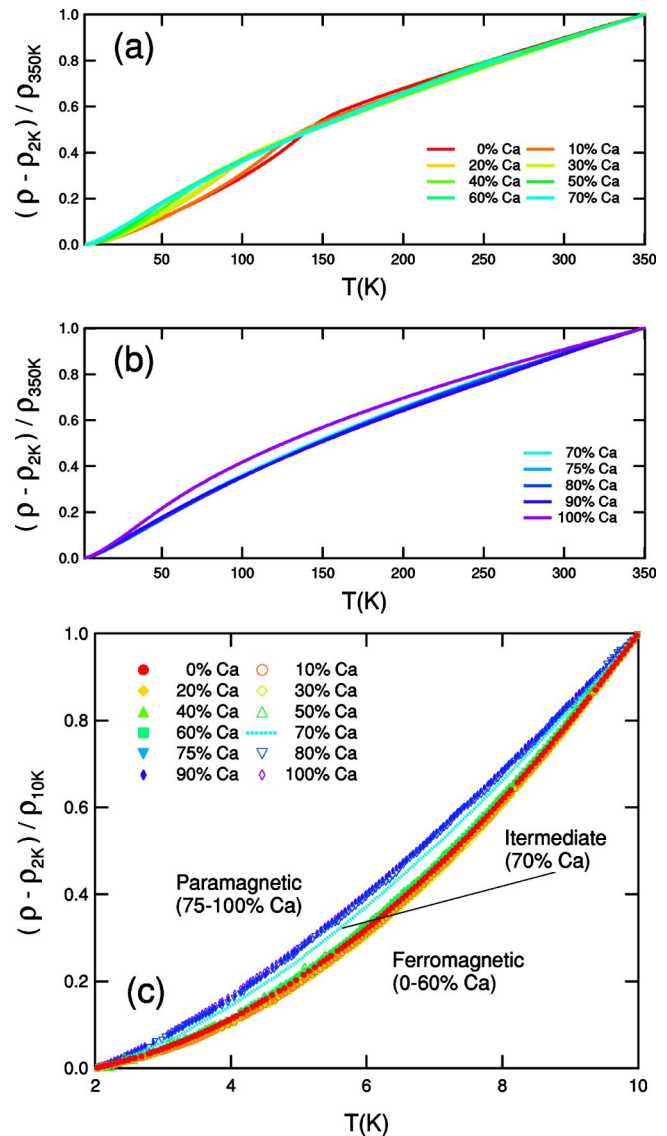


FIG. 3. (Color online) (a) Normalized resistivities for 0–70 % Ca. (b) Normalized resistivities for 75–100 % Ca. The resistance of the 60% Ca sample (dotted line) is shown for comparison. (c) Scaled resistivities in the 2–10 K range showing the different scalings of the ferromagnetic and paramagnetic samples.

the downturns in the resistivity curves show monotonic compositional variation.

This compositional variation ceases for the nonmagnetic samples ($0.75 \leq x \leq 0.90$), indicating that there are no significant differences in the spin scattering between these compositions [Fig. 3(b)]. The failure of the 100% Ca sample to scale with the other nonmagnetic samples is a consequence of the higher RRR of this sample rather than intrinsic electronic differences. This can be seen in Fig. 3(c), where the data are renormalized to highlight the low temperature (2–10 K) variations of the resistivity, which reflect the the intrinsic electronic interactions. The low temperature scaling of our $\text{Ca}_x\text{Sr}_{1-x}\text{RuO}_3$ samples shows that the resistivities of the entire compositional range collapse onto two primary curves. The nonmagnetic samples ($0.75 \leq x \leq 1.00$) fall on

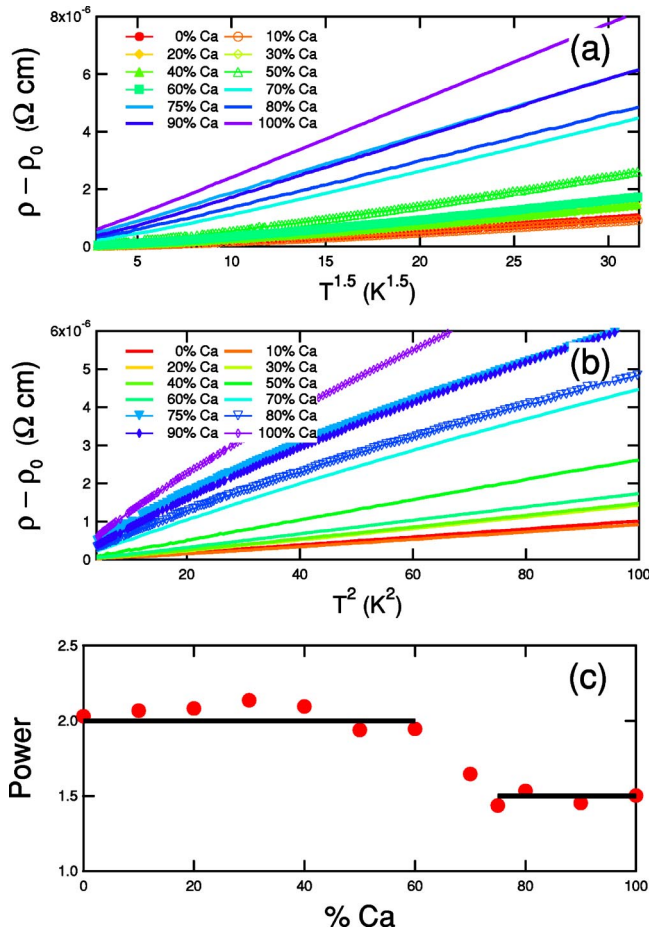


FIG. 4. (Color online) (a) Intrinsic resistivity plotted as a function of T^2 . (b) Intrinsic resistivity plotted as a function of $T^{1.5}$. (c) Resistivity power (α in $\rho = \rho_0 + AT^\alpha$) as a function of Ca concentration. Solid lines are drawn at $\alpha = 1.5$ and 2.0 .

the more slowly varying curve and the ferromagnetic ($0.00 \leq x < 0.70$) ones fall on the more rapidly varying curve. The only exception is the weakest ferromagnet ($x = 0.70$), which falls on an intermediate curve. This establishes the low temperature regime of 2–10 K as the proper regime for looking for scaling exponents and other quantum critical phenomena. It should be noted that this temperature regime has also been shown to be the most significant one for understanding the related ruthenates $\text{Sr}_3\text{Ru}_2\text{O}_7$ (Ref. 4) and $\text{Ca}_{2-x}\text{Sr}_x\text{RuO}_4$.²⁰

One hallmark of non-Fermi-liquid behavior is power law scaling of resistivity, of the general form $\rho = \rho_0 + AT^\alpha$, where α is a number less than the normal value of 2 predicted by Landau theory. In principle, the exponent α can give insights into the nature of a system, via comparison with theoretical predictions.⁹ In the framework of the spin fluctuation theories of Moriya and Takimoto²¹ and Lonzarich,²² resistivity is predicted to scale as $T^{5/3}$ in the vicinity of a three dimensional ferromagnetic transition. This can be contrasted to the antiferromagnetic case, which is instead predicted to show a $T^{3/2}$ dependence. CaRuO_3 was previously reported to obey $T^{3/2}$ scaling in its resistivity^{7,8} over the range of 2–10 K.

Log-log plots of the normalized resistivity ($\rho - \rho_0$) versus temperature showed nearly linear behavior below 10 K over

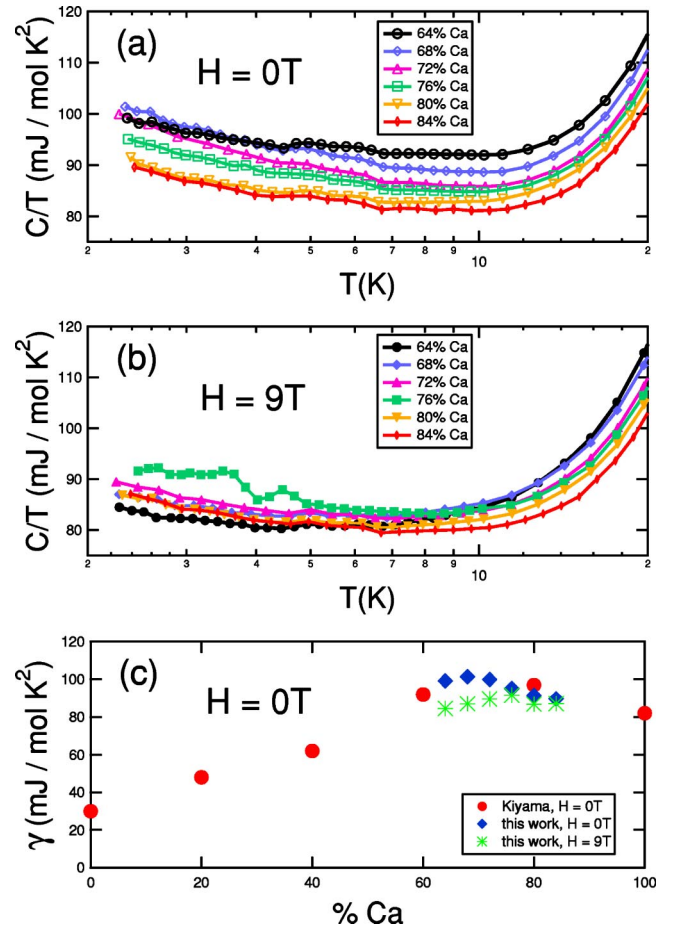


FIG. 5. (Color online) (a) Zero-field C/T data, demonstrating $C/T \sim \log_{10} T$ below 7 K. (b) High-field ($H = 9 \text{ T}$) C/T data. Note the generally lower magnitudes of C/T . (c) Electronic contributions, γ , to C/T . In this work, γ values are taken from the measured C/T at the lowest temperature studied ($\sim 2 \text{ K}$). The values reported by Kiyama *et al.* were obtained by extrapolations to $T = 0$, with the different methods potentially causing the discrepancy in the 80% Ca data.

our entire range of $\text{Ca}_x\text{Sr}_{1-x}\text{RuO}_3$ samples, again confirming that the search for power laws should be done in this regime (data not shown). As seen in Fig. 4(a), normal Fermi-liquid behavior (T^2 scaling) is observed for samples with $< 70\%$ Ca. On the other hand, samples with $\geq 75\%$ Ca are found to scale as $T^{1.5}$ [Fig. 4(b)]. The 70% Ca sample is again found to fall in an intermediate crossover regime, as seen when the extracted resistivity power law exponents are plotted in Fig. 4(c). This convincingly demonstrates two important facts. First, the nature of the conduction is fundamentally different in the magnetic and nonmagnetic samples. Second, the scattering processes must be fundamentally the same for each of the individual samples within each class of samples (ferromagnetic and paramagnetic). From this, we conclude that the most ferromagnetic samples are behaving as Fermi liquids, while the *entire* range of nonmagnetic samples exhibit the same type of non-Fermi-liquid behavior originally reported for the end member, CaRuO_3 . This is important to note as disorder has often been invoked as a necessary component of NFL behavior. However, the same NFL scaling of the resis-

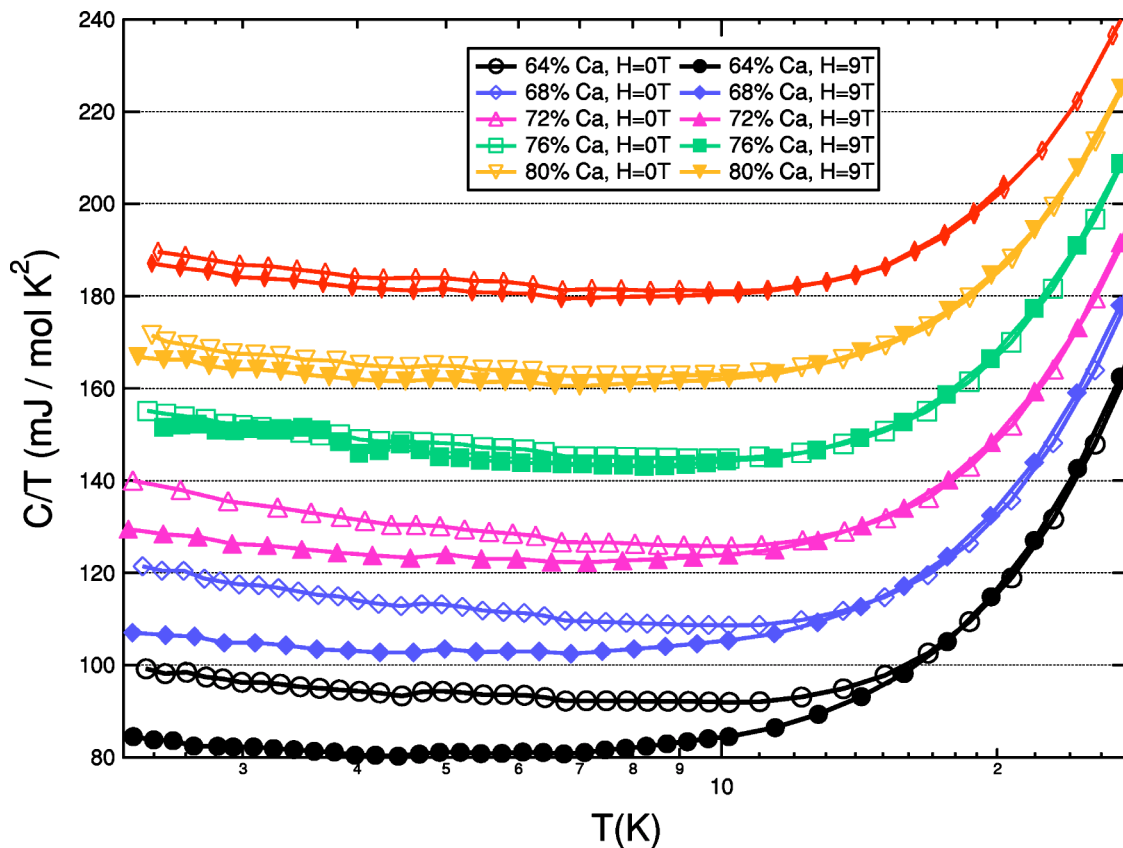


FIG. 6. (Color online) Comparison of the zero-field (open symbols) and high-field (solid symbols) specific heats of compositions near the quantum phase transition in $\text{Ca}_x\text{Sr}_{1-x}\text{RuO}_3$, demonstrating the significant spin fluctuation effects for 64–72 % Ca. Successive Ca concentrations greater than 64% Ca are offset by an extra 20 mJ/mol K^2 per step.

tivity data is observed both for the single phase (CaRuO_3 , $x=1$) and solid solution ($\text{Ca}_x\text{Sr}_{1-x}\text{RuO}_3$, $0.75 \leq x < 1$) films studied here, indicating that crystalline disorder is of minimal importance in these samples.

Compounds exhibiting Fermi-liquid behavior are expected to have a heat capacity of $C = aT^3 + \gamma T$ due to the phononic and electronic contributions, respectively. The zero-field ($H=0$ T) and high-field ($H=9$ T) specific heat data for a range of compositions near the quantum phase transition ($x=0.64, 0.72, 0.76, 0.80$, and 0.84) are shown in Fig. 5. At low temperatures where the phononic contribution is negligible, Fermi-liquid theory predicts C/T to have a constant value. This is not observed in the $\text{Ca}_x\text{Sr}_{1-x}\text{RuO}_3$ samples, which instead have a minimum in C/T plots around 10 K. As temperatures are decreased below 10 K, C/T continues to increase with no apparent trend toward saturation. This non-Fermi-liquid behavior is most prevalent near the ferromagnetic quantum phase transition in the $\text{Ca}_x\text{Sr}_{1-x}\text{RuO}_3$ system, as seen in Fig. 5(a) and also in previous measurements.¹⁵ The γ values exhibits a maximum near this QPT [Fig. 5(c)], with the γ for $x=0.72$ exceeding 100 mJ/mol K^2 , more than three times higher than that of pure SrRuO_3 . As seen in Figs. 5(b) and 6, the application of strong magnetic fields suppresses the electronic portion of the specific heat by 10–15 mJ/mol K^2 for samples with $x=0.64$ to 0.72, indicating that spin fluctuations play an important role at these concentrations. These spin fluctuations

are only contributing near the QPT, as both samples with higher Ca contents (Fig. 6) and pure SrRuO_3 (Ref. 15) have heat capacities which are field-independent.

Specific heat data provide additional evidence for quantum critical scaling at the quantum phase transition in the $\text{Ca}_x\text{Sr}_{1-x}\text{RuO}_3$ system. One of the recognized hallmarks of quantum criticality is a $\log_{10} T$ dependence of C/T .^{9,11} In plots of the zero-field ($H=0$ T) specific heats versus $\log_{10} T$ [Fig. 5(a)], the entire range of $\text{Ca}_x\text{Sr}_{1-x}\text{RuO}_3$ samples studied exhibit linearity up to approximately 7 K. The compositions nearest the QPT ($x=0.68, 0.72$) have the strongest temperature dependence in addition to having largest low temperature γ values. This linearity is muted for the high-field data [Fig. 5(b)], where the upturns in C/T below 10 K result in an increase of only ~ 5 mJ/mol K^2 .

In conclusion, both resistivity and specific heat data indicate that the non-Fermi-liquid behavior of CaRuO_3 results from its proximity to the quantum phase transition where the ferromagnetic moment of SrRuO_3 is suppressed. The NFL behavior that was initially reported for CaRuO_3 is not unique to that composition, but is instead a universal feature of the $\text{Ca}_x\text{Sr}_{1-x}\text{RuO}_3$ phase space with $0.75 < x < 1$. The NFL resistivity exponent of $T^{1.5}$ found for $\text{Ca}_x\text{Sr}_{1-x}\text{RuO}_3$ samples is the same one observed when pressure is used to suppress the itinerant electron ferromagnetism of MnSi , and has also been reported for two other itinerant ferromagnets, ZrZn_2 and Ni_3Al .¹³ Given the widely disparate nature of the

$\text{Ca}_x\text{Sr}_{1-x}\text{RuO}_3$ films and the MnSi single crystals (oxide versus intermetallic compositions, epitaxial films versus single crystals, residual resistivities of a few hundreds versus a few tenths of $\mu\Omega$ cm, doping levels of up to 25% versus a pure system, strong versus weak crystalline electrical field effects), it is intriguing that such similar behaviors are observed, and is indicative of the dominant role that the nearly magnetic itinerant electrons play in determining the behavior of these systems.

The helpful advice on experimental techniques from B. Sales, R. Jin, and J. Thompson was greatly appreciated, as was the theoretical guidance of A. Millis, D. Singh, and R. Osborn. Special thanks go to V. Keppens and G. Petculescu for making equipment at the University of Mississippi available for exploratory measurements. Research was sponsored by the U.S. Department of Energy under Contract No. DE-AC05-00OR22725 with the Oak Ridge National Laboratory, managed by UT-Battelle, LLC.

-
- ¹Y. Maeno, H. Hashimoto, K. Yoshida, S. Nishizaki, T. Fujita, J. G. Bednorz, and F. Lichtenberg, *Nature (London)* **372**, 532 (1994).
- ²J. G. Bednorz and K. A. Muller, *Z. Phys. B: Condens. Matter* **64**, 189 (1986).
- ³P. Khalifah, K. D. Nelson, R. Jin, Z. Q. Mao, Y. Liu, Q. Huang, X. P. A. Gao, A. P. Ramirez, and R. J. Cava, *Nature (London)* **411**, 669 (2001).
- ⁴S. A. Grigera, R. S. Perry, A. J. Schofield, M. Chiao, S. R. Julian, G. G. Lonzarich, S. I. Ikeda, Y. Maeno, A. J. Millis, and A. P. Mackenzie, *Science* **294**, 329 (2001).
- ⁵P. Khalifah, R. Osborn, Q. Huang, H. W. Zandbergen, R. Jin, Y. Liu, D. Mandrus, and R. J. Cava, *Science* **297**, 2237 (2002).
- ⁶S. Nakatsuji and Y. Maeno, *Phys. Rev. Lett.* **84**, 2666 (2000).
- ⁷L. Klein, L. Antognazza, T. M. Geballe, M. R. Beasley, and A. Kapitulnik, *Physica B* **261**, 431 (1999).
- ⁸L. Capogna, A. P. Mackenzie, R. S. Perry, S. A. Grigera, L. M. Galvin, P. Raychaudhuri, A. J. Schofield, C. S. Alexander, G. Cao, S. R. Julian, and Y. Maeno, *Phys. Rev. Lett.* **88**, 076602 (2002).
- ⁹G. R. Stewart, *Rev. Mod. Phys.* **73**, 797 (2001).
- ¹⁰C. L. Seaman, M. B. Maple, B. W. Lee, S. Ghamaty, M. S. Torikachvili, J.-S. Kang, L. Z. Liu, J. W. Allen, and D. L. Cox, *Phys. Rev. Lett.* **67**, 2882 (1991).
- ¹¹H. von Lohneysen, *J. Phys.: Condens. Matter* **8**, 9689 (1996).
- ¹²C. Pfleiderer, G. J. McMullan, S. R. Julian, and G. G. Lonzarich, *Phys. Rev. B* **55**, 8330 (1997).
- ¹³C. Pfleiderer, S. R. Julian, and G. G. Lonzarich, *Nature (London)* **414**, 427 (2001).
- ¹⁴C. B. Eom, R. J. Cava, R. M. Fleming, J. M. Phillips, R. B. Vandover, J. H. Marshall, J. W. P. Hsu, J. J. Krajewski, and W. F. Peck, *Science* **258**, 1766 (1992).
- ¹⁵T. Kiyama, K. Yoshimura, K. Kosuge, H. Michor, and G. Hilscher, *J. Phys. Soc. Jpn.* **67**, 307 (1998).
- ¹⁶P. Khalifah and D. Mandrus (unpublished).
- ¹⁷S. Hyun, J. H. Cho, A. Kim, J. Kim, T. Kim, and K. Char, *Appl. Phys. Lett.* **80**, 1574 (2002).
- ¹⁸A. P. Mackenzie, J. W. Reiner, A. W. Tyler, L. M. Galvin, S. R. Julian, M. R. Beasley, T. H. Geballe, and A. Kapitulnik, *Phys. Rev. B* **58**, R13 318 (1998).
- ¹⁹L. Klein, J. S. Dodge, C. H. Ahn, J. W. Reiner, L. Mioeville, T. H. Geballe, M. R. Beasley, and A. Kapitulnik, *J. Phys.: Cond. Matter* **8**, 10111 (1996).
- ²⁰S. Nakatsuji, D. Hall, L. Balicas, Z. Fisk, K. Sugahara, M. Yoshioka, and Y. Maeno, *Phys. Rev. Lett.* **90**, 137202 (2003).
- ²¹T. Moriya and T. Takimoto, *J. Phys. Soc. Jpn.* **8**, 960 (1995).
- ²²G. G. Lonzarich, in *The Electron*, edited by M. Springford (Cambridge University Press, Cambridge, 1997), Chap. 6.